INTERNATIONAL JOURNAL OF HYDROGEN ENERGY 40 (2015) 6661–6671

Available online at www.sciencedirect.com

ScienceDirect

journal homepage: www.elsevier.com/locate/he

Investigating the influence of Pd situation (as core or shell) in synthesized catalyst for ORR in PEMFC

*M. Javaheri**

Ceramic Department, Materials and Energy Research Center, Karaj, Iran

ARTICLE INFO

Article history:
Received 19 November 2014
Received in revised form
27 February 2015
Accepted 7 March 2015
Available online 15 April 2015

Keywords:
Core-shell
Catalyst
Fuel cell
Ru
Pt
Pd

ABSTRACT

Two series of Pd@Pt (Pd as core and Pt as shell) and Ru@Pd–Pt (Ru as core and Pt–Pd as shell) core-shell structures with different molar ratio of metals on Vulcan were prepared by a successive reduction procedure. The effect of Pd as core (Pt as shell) is compared with the effect of Pd–Pt alloy as shell (Ru as core) for oxygen reduction reaction (ORR). The physical properties of the synthesized catalysts are characterized by inductive coupled plasma (ICP), X-ray diffraction (XRD), transmission electron microscopy (TEM). The results of half-cell testing indicated that the synthesized catalysts activity for ORR is better than commercial Pt/C. Despite low catalyst loading (0.3 $mg.cm^{-1}$), polarization behavior in the single cell testing also suggests that the Ru@Pd–Pt has a much better performance than the Pd@Pt catalyst. This good efficiency can be attributed to the effect of Ru on electronic properties of Pt and the positive effect of Pd as alloyed with Pt, increasing adsorption and reduction of O_2 on Pt–Pd.

Introduction

Polymer electrolyte fuel cell (PEMFC) has great potential to be used in both stationary power generation and vehicular power sources [1]. Platinum has a wide range of catalytic applications due to its unique chemical and physical characteristics [2–5]. The catalyst usually reduced on carbon support, the carbon support material has been pretreated in order to improve the electrocatalytic activity [6]. However, the most critical problem for Pt catalysts is high cost because of the limited supply. Pt-based electro catalysts are usually employed in PEMFC as cathode electro catalysts for ORR at relatively low temperatures [7]. Currently, the major challenge in this field is to reduce the fuel cell energy cost by developing low cost materials, processes and components [8]. Bimetallic nanocrystals consisting of two distinct metals such as Pt–Ru, Pt–Pd etc., are attractive for a wide variety of catalytic and electro catalytic applications as they can exhibit not only a combination of the properties associated with both metals, but also enhancement or synergy due to a strong coupling between the two metals [9,10]. To maximize the efficiency of Pt particles, the ideal structure of a Pt-based catalyst should consist of the total available Pt atoms distributed on the electrochemical reaction interface. Based on this consideration, the core–shell nanostructure is expected to effectively increase the utilization efficiency of precious metal electro catalysts [11]. Hence, replacing the core of the nanoparticles of electro catalysts with less expensive or non-precious metals and/or by producing Pt nanosphere shells with high surface to volume ratios, gives us a chance to increase the catalytic activity and

* Tel.: +98 912 5263035.
E-mail addresses: m.javaheri@merc.ac.ir, javaheri54@yahoo.com.
http://dx.doi.org/10.1016/j.ijhydene.2015.03.030

utilization efficiency of Pt electro catalysts. This structure would consequently lower the required Pt loading, reducing production expenses [12–20].

Recently, many researches have focused on the synthesis of core–shell catalytic structures to be applied in PEM fuel cells. In 2013, a number of reports were published on the synthesis of Pt as shell on commercial Pd/C with different molar ratios and the ORR on the surface of the catalyst was investigated. The studies revealed that the activity of this catalyst was better than the commercial Pt/C and Pd/C [21]. H. Wang et al. [22] prepared the Pd@Pt core–shell nanowire array using an anodized aluminum oxide template with electro deposition and magnetron sputtering method. The obtained results indicated that this catalyst was highly active toward the electro oxidation of methanol in acid medium for DMFCs in comparison with that of conventional Pt–Ru supported carbon (Pt–Ru/C) electro catalysts. In 2012 [23], the Pt–Pd core–shell structure was synthesized and mass activity of this catalyst was compared with commercial Pt/C. L. Zhang et al. [24] studied the anode of PEMFC and reported that the overall performance of core–shell catalyst (Ru@Pt/Ti_4O_7) in the presence of CO at various concentrations was significantly higher than that of Pt Ru/C alloy catalyst. The Pd–Au hollow structures were observed to be suitable cores for Pt in ORR, being capable of enhancing the performance of fuel cell [25]. M. Y. Duan et al. [26] synthesized the Au@Pt catalyst for methanol electro oxidation where the results show that this catalyst has higher performance than commercial Pt/C. The core-shell structure of Fe@Pt/SWNT was prepared by K. Shimizu et al. [16]. This catalyst enhanced the ORR in comparison with the commercial catalyst. The Ru@Pt_x Pd_y/C core–shell structure were synthesized and applied for formic acid oxidation. The higher electro catalytic activity toward formic acid oxidation on the core–shell structure of Ru@Pt_x Pd_y/C catalyst than that on Pt_x Pd_y/C suggests the high utilization of noble metals [27].

Most studies refer to the catalytic activity of Ru on ORR, but fewer on Pt, in acid or alkaline electrolyte [28,29]. Theoretical and experimental research represented the positive effect of Ru on the electronic properties of Pt and consequent enhancement the Pt activity for ORR [31–33]. In addition, Pd can improve the electro catalytic activity of Pt for ORR [34–36].

In this work, core–shell catalyst structures were prepared by the synthesis of 2 series of catalysts through impregnation with hydrothermal method. The first series contained Pd as core and Pt as the shell part, while the second one included Ru as core and Pt–Pd as the shell. The effect of molar ratio on the electrode performance for ORR was investigated. A rolling technique was employed to prepare the gas diffusion electrode (GDEs) with three layer structures.

Experimental

Catalyst synthesis

First, adequate amount of Vulcan (Cabot) was refluxed in H_2O_2 30% (Merck) and HNO_3 10% (Merck) with volume ratio 1:3 at 80 °C for 6 h. Carbon powder was removed using centrifugal (ROTINA 46) and washed by distilled water. Then, the pretreated carbon was dried at 80 °C for 12 h.

Dispersion of catalyst with core–shell structure was carried out step by step. In the first step, the core seeds were dispersed on Vulcan powder and thereafter the shell was dispersed on the core. To prepare Ru/C, the $RuCl_3.3H_2O$ precursor was dissolved in diluted HCl. Since the molar ratio of Ru and Pt–Pd was different (Table 1), the pretreated Vulcan was divided in to 3 parts. Each part was mixed with precise amount of the $RuCl_3$ solution and prepared suspensions were allowed to evaporate in 70 °C. Finally, in order to complete reduction of Ru on Vulcan, the powder was heated in furnace at 200 °C under H_2 atmosphere. The Ru/C was synthesized with three different molar ratios (Table 1).

To prepare Ru@Pt–Pd/C, appropriate amount of $PdCl_2$ and $H_2PtCl_6.6H_2O$ with sodium citrate were dissolved in ethylene glycol and then steered for 1 h to completely dissolve sodium citrate. Subsequently, the synthesized Ru/C was added to the mixture and the pH was adjusted up to 10 by drop-wise addition of KOH in ethylene glycol into solution under steering. The mixture was then transferred into a Teflon-lined autoclave and conditioned at 130 °C for 6 h, followed by centrifuging, washing, and vacuum drying at 70 °C [27].

Although the preparation of Pd@Pt included the second step mentioned in the preceding paragraph, in this step Pd was reduced on the pretreated Vulcan and then $H_2PtCl_6.6H_2O$ with sodium citrate was used as the precursor of catalyst in the shell.

Hereinafter, the synthesized catalysts were labeled by 3 integers that indicated the molar ratio of Pt, Ru and Pd, respectively (Series 1 include 211, 231 and 432. Series 2 include 101,102,103).

GDEs fabrication

To fabricate the three-layer GED, the diffusion layer, a mixture of 30 wt% PTFE and 70 wt% Vulcan in 2-propanol (Merck), water, and glycerol (Merck) was sonicated for 20 min with a sonicator (Sonoswiss SW3H) to produce a homogeneous suspension. Diffusion layer was made hydrophobic to avoid flooding in their bulk. The suspension was then rolled onto the carbon paper (TGPH-0120T) (Toray) and dried in air at 120 °C for 1 h. The prepared electrode was finally sintered at 340 °C for 30 min. Loading of the micro porous layer was fixed at 1 mg cm^{-2} [37,38].

To prepare the catalyst layer of GDEs, a homogeneous suspension containing the desired amounts of the

Table 1 – Name and molar ratio of synthesized catalyst.

Catalyst no.		1	2	3	4	5	6
Name		231	432	211	103	102	101
Pt:Ru:Pd		2:3:1	4:3:2	2:1:1	1:0:3	1:0:2	1:0:1
Precursor	%Pt	32.5	44.5	50	25	33.5	50
	%Ru	50	33.5	25	0	0	0
	%Pd	17.5	22	25	75	66.5	50
ICP	%Pt	38	48	53.1	23.6	31.5	43
	%Ru	46.2	31.4	25.8	0	0	0
	%Pd	15.8	20.6	21.1	76.4	68.5	57

synthesized catalyst (7 wt.%), Nafion solution (5% from Aldrich), 2-propanol, water, and glycerol was sonicated for 20 min. The suspension was subsequently rolled onto the diffusion layer. The obtained electrode was dried at 40 °C for 30 min and then 80 °C for 30 min. The catalyst loading was 0.2 mg cm^{-2}.

Electrode fabrication for single cell

For the single cell, a three-layer electrode was fabricated through the same steps as those used for the fabrication of GDEs (previous section). In this study, the best catalyst of each series was used as the cathode catalyst, while the commercial Pt/C (10% wt) was used as the anode catalyst. The electrode area and catalyst loading value were considered to be 5 cm^2 and 0.3 mg cm^{-2}, respectively.

Physical properties

A transmission electron microscope (CM Philips 30) was used to prepare TEM images. The X-ray diffraction (XRD) technique was employed for the synthesized catalysts using a Philips pw3710 diffractometer with a Cu X-ray source operating at 40 kV and 40 mA. The XRD patterns were obtained at a scanning rate of 1°/min with a step size in the 2θ scan of 0.02° in the 20–90° range.

The amount of reduced Ru, Pd and Pt on each support was determined through the application of inductive coupled plasma (ICP) technique (ICP-AES, 314, Switz). In order to conduct these measurements, 5 mg of each sample (synthesized catalyst) was dissolved in a mixture of hydrochloric acid and nitric acid (3/1). These solutions were refluxed at 70 °C in advance of being used in the ICP measurements.

Electrochemical measurement

For electrochemical tests, an EG&G Princeton Applied Research Model 2273 instrument was used to determine the electrochemical properties of the electrodes. The performances of the porous GDEs (geometric exposed area 1 cm^2) in the reduction of oxygen were investigated in 0.5 M H_2SO_4. All measurements were performed at 25 °C in a conventional three-electrode cell, with O_2 flowing at 50 mL min^{-1} for linear sweep voltammetry (LSV), Chronoamperometry, and impedance spectroscopy and Ar flowing for cyclic voltammetry (CV) and ionic resistance measurement. The GDEs were mounted into a Teflon holder containing a graphite disk as current collector and providing oxygen feed from the back of the electrode. An Ag/AgCl reference electrode was placed close to the working electrode surface, while a large area platinum flat electrode was employed as the counter electrode. In order to perform a quantitative evaluation of resistance against the ORR, the AC electrochemical impedance spectroscopy (EIS) method was used. In the Nyquist plot of the semicircle diameter, R_p is the polarization resistance and the sum of the electrode and electrolyte resistance that was subtracted for these GDEs. The polarization resistance was the sum of two terms: the charge transfer and diffusion resistances. Impedance measurement was investigated in 0.4 V vs Ag/AgCl potential for obtaining R_p. This potential was in ohmic resistance region. The AC potential amplitude was 5 mV and the frequency range was in the10 kHz–0.1 Hz interval. We used impedance measurements to characterize the ionic resistances of the electrodes. At low frequencies, a Warburg-like response (45° slope) was observed which indicated the occurrence of ion migration through the catalyst layer. The ionic resistance R_{ion} could be obtained from the length of the Warburg-like region projected onto the real impedance (Z_{real}) axis [39–41]. To obtain R_{ion}, the impedance measurement was investigated in OCV potential (10 kHz–0.1 Hz) and Argon-bathed. Finally, the best catalysts of each series were used as the cathode catalyst in single cell and the cells performance was tested. The performance of the MEAs was characterized by polarization curves and EIS. Polarization curves were obtained by sweeping the cell voltage from OCV to 250 mV with the scan rate of 5 mV s^{-1}. The polarization curves obtained during activation time allow the evaluation of the potential history and power density as a function of the current and provide a clear insight into the evolution and quantification of the fuel cell performance. The impedance spectra were also recorded at 10 points per decade over the frequency range of 10 kHz–10 mHz. The amplitude of the AC signal was kept at 5% of the DC current. The Nyquist plots were recorded at 0.3 V.

Result and discussion

The electrochemical reaction in GDE occurs in a three-phase zone which includes the reactant (gas phase), electrons (solid phase), and protons (liquid phase) [42]. Therefore, increasing the triple phase zone improves the electrode quality and consequently the cell performance. It is expected that the core-shell structure of catalyst will increase the triple phase zone.

Physical characterization of catalyst

The catalysts were synthesized as mentioned in the experiment section.

The ICP results indicated that the samples contained 7 wt% catalysts (instead of the 10 wt% based on precursor). The percentage of synthesized catalysts is listed in Table 1, the percentages of which are in relation with each other not with the precursor catalysts.

The XRD pattern of series 1 and 2 are presented in Fig. 1A and B. The peak centering at 24.5° for all the catalysts could be ascribed to the carbon support. There were four observable peaks at 2θ angles of ca. 40°, 47°, 68° and 81° for Pt plates (111), (200), (220), and (311), respectively. The broadening of peaks indicates that the catalyst particles are of nanometer scale (Table 2). The averages size of the catalyst particles was calculated from the line broadening of the (111) peak by using the Scherrer equation after background subtraction and found to be nanometer-sized (Table 2):

$$d = \frac{0.9\lambda}{B_{2\theta}\cos\theta} \quad (1)$$

where d is the average particle size, λ is the wavelength of the X-ray (1.54056A), θ is the angle at the maximum of the peak, and $B_{2\theta}$ is the width of the peak at half-height.

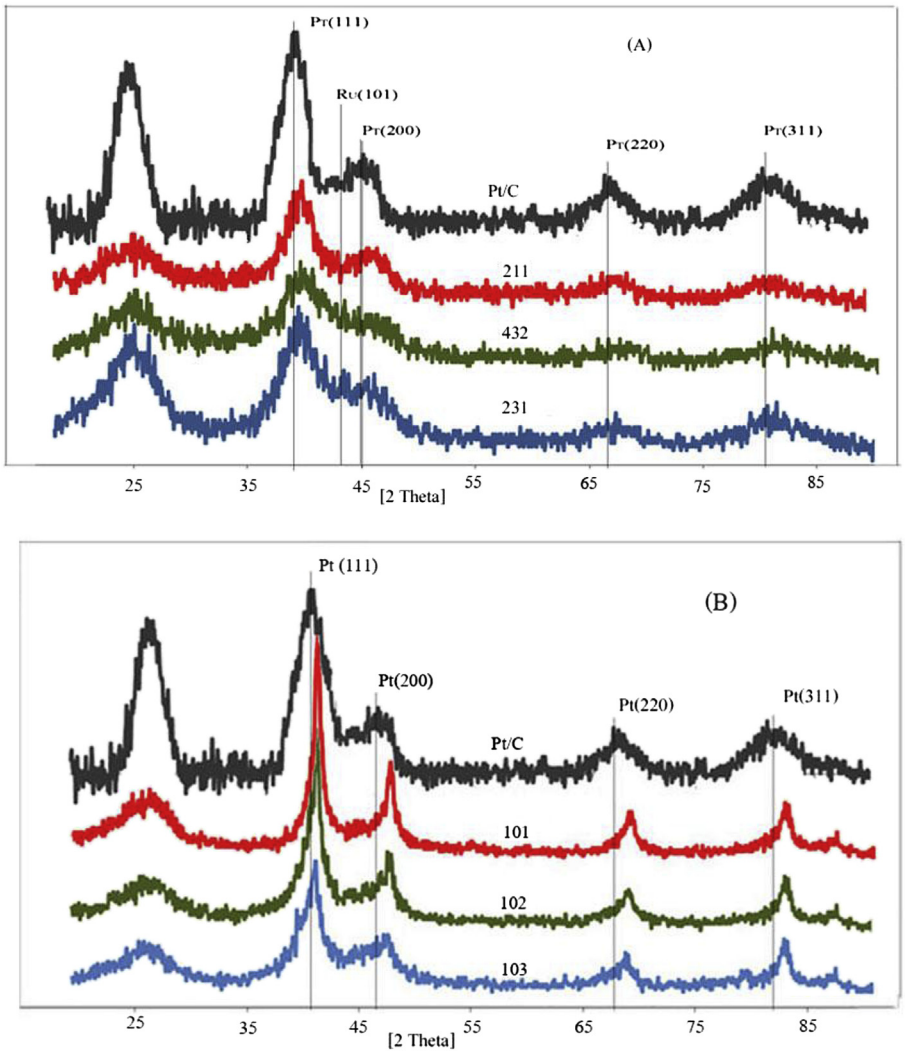

Fig. 1 – XRD pattern (A) catalyst series 1 (Ru@Pt–Pd) and (B) catalyst series 1 (Pd@Pt).

If the nanoparticles could be well dispersed on carbon substrate, the triple phase zone could be expanded and the electrode performance could be improved. In contrast with the commercial Pt/C, the XRD pattern of series 1 synthesized catalyst (Ru@Pd–Pt) contains a weak peak at around 43°. This peak is related to Ru (101) and gradually became weaker by reducing the amount of Ru. This phenomenon is attributed to the coverage of Ru particles with Pt–Pd (in series 1), being capable of forming a core-shell structure [21,43,28]. The presence of the Ru (101) peak reveals that Ru has not been alloyed with Pt–Pd. In fact, in case of alloy formation, Ru atoms would enter the fcc structure, while the introduction of Ru into the hcp structure would be eliminated and consequently remove the Ru (101) peak from the XRD pattern [44].

Table 2 – Exchange current density, tafel slop, transfer coefficient, current density at 0.3 V, diffusion coefficients, charge transfer resistances, ionic resistances and particle size of all fabricated GDEs.

GDE	$i_0 \times 10^{-5}$ (A cm^{-2})	b (mV de^{-1})	α_c	i at 0.3(V) (mA mg_{cat}^{-1})	EAS (m^2 g_{cat}^{-1})	Rf	$D^{1/2} \times C^* \times 10^{-8}$ (Mol. Cm^{-2} $s^{-1/2}$)	R_p(ohm)	1/3 R_{ion} (ohm)	d(nm)
231	29.12	43.58	1.36	1002.78	174.36	1.430	32.73	0.999	1.09	2.4
432	16.51	53.45	1.10	636.90	117.92	1.303	29.33	2.32	2.35	2.2
211	14.36	59.40	0.99	639.74	136.45	1.99	28.22	2.10	4.48	2.1
103	9.17	47.07	1.25	1018.01	52.54	0.449	33.71	0.912	1.41	2.3
102	6.23	54.79	1.07	542.75	40.05	0.314	23.03	3.47	5.57	3.1
101	8.02	49.28	1.19	806.74	39.52	0.296	24.65	1.38	1.73	4.1
Pt/C	7.45	49.12	1.13	653.51	12.7	–	23	4.73	–	5

The XRD results also indicate that the presence of Ru core has affected the position and d-spacing of the Pt peaks where a positive shift appeared and the d-spacing was reduced. For example, the 2θ angles of Pt (111) changed from 39.35° in Pt/C to 39.77° in 231 (series 1) and d-spacing decreased from 2.3 in Pt/C to 2.26° in 231. Since the lattice parameter of Pd is very close to that of Pt, the only subtle difference for the XRD pattern of the Pt–Pd alloy in shell is the peak position with respect to Pt/C pattern.

In series 2, in the presence of Pd nanoparticles, since the lattice parameter of Pd is very close to that of Pt and the employed agent is a relevant mild reducing agent [21], Pt is prone to seed and grow on Pd nanoparticles instead of on the carbon black. Thus, the Pd–Pt/C catalyst can be considered as a (Pd@Pt) core-shell structure. Because Pt and Pd have the same crystal structure (fcc) and very close lattice parameters, the sets of diffraction peaks of Pt and Pd are overlapped. Furthermore, we observed that the peaks (e.g., see (220)) of Pt@Pd/C are located between that of commercial Pd/C (~68.02° [21]) and commercial Pt/C (66.86° Fig. 1B) which is consistent with the results of core–shell structured nanoparticles reported in literature where the diffraction peaks of core–shell structures is located between the individual core and shell metals [45,46].

The TEM images of series 1 demonstrated that the particle size of the catalyst is nanometer-sized. Proper dispersion of nanoparticle can cause the expansion of the three-phase zone, improving the performance of catalyst in ORR. It can be observed that the nanoparticles of catalyst are dispersed on the carbon support in sphere-like shapes. The comparison of TEM images of 211 and 231 catalyst (Fig. 2A and B) show that in 231, the catalyst nanoparticle are smaller and more efficiently dispersed on carbon. The electrochemical results emphasize that the active sites are better formed in 231. However, in 211, the agglomeration of catalyst nanoparticles would result in an increase in particle size and consequently decrease the electrochemical active surface area and performance of the layer. The reduction in the surface activity of the fabricated electrode is confirmed by the electrochemical results, emphasizing that the molar ratio 2:3:1 of Pt:Ru:Pd had better performance than the other catalysts (Table 2). Based on the TEM images of 103 and 102 (Fig. 2C and D), the 103 nanoparticles have been well dispersed on the carbon support, whereas the 102 nanoparticles have agglomerated. Thus, it can be concluded that the 1:0:3 M ratio of Pt:Ru:Pd had better performance for ORR rather than the other molar ratios in series 2 (Table 2).

Considering the electrochemical results of GDEs, changing the molar ratio of core and shell will affect the electrochemical behavior of electro active species on the electrode surface.

Cyclic voltammetry of gas diffusion electrodes

Cyclic voltammetry was employed to measure the electro active surface area (Fig. 3A–C). Also, the columbic charge for hydrogen desorption was used to calculate the electro active surface area (EAS) of each electrode (Table 2) [47]:

$$EAS = \frac{Q_h}{0.21 \times [catalyst]} \quad (2)$$

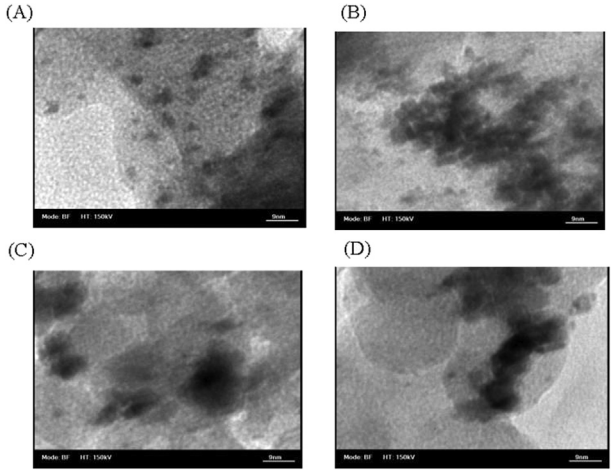

Fig. 2 – TEM image of Ru@Pt–Pd (A) catalyst 231 (2:3:1 of Pt:Ru:Pd), (B) catalyst 211 (2:1:1 of Pt:Ru:Pd) and Pd@Pt (C) catalyst 103 (1:0:3 of Pt:Ru:Pd), (D) catalyst 102 (1:0:2 of Pt:Ru:Pd).

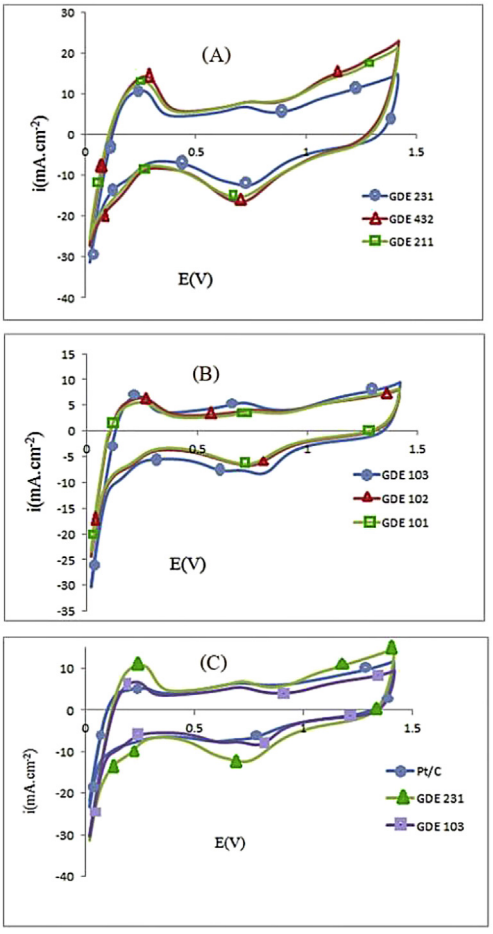

Fig. 3 – Cyclic voltammetry of (A) series 1 electrode (Ru@Pt–Pd) (231, 432, 211), (B) series 2 electrodes (Pd@Pt) (103, 102, 101) and (C) the comparison (Pt/C, 231, 103) in 0.5 M H_2SO_4, argon atmosphere, 50 mV s^{-1} scan rate and 25 °C.

where Q_h is the charge for hydrogen desorption (mC cm^{-2}), [catalyst] is the catalyst loading (mg cm^{-2}) and 0.21 (mC cm^{-2}) is the charge required to oxidize a monolayer of H_2 on bright catalyst. The roughness factor (R_f) can then be calculated by using the following equation:

$$R_f = \frac{EAS}{s} \tag{3}$$

where S is the geometric surface area (m^2 g^{-1}). These catalysts demonstrate the adsorption-desorption peak, confirming the activation of the catalyst. The active surface area of catalysts was tabulated in Table 2. The achievement of high active surface area could be attributed to the formation of the three-phase zone. According to the EAS results, the performance of GDE for ORR is enhanced due to the expansion of the three-phase zone.

Kinetic parameter of electrodes

The kinetic parameters of GDEs are important to determining the activation of these for ORR. The analysis of the experimental polarization data was performed using the Tafel equation [48]:

$$\eta = E - E_{eq} = -\frac{2.303RT}{nF\alpha}\log\frac{i}{i_0} \tag{4}$$

where η is the overpotential, E_{eq} is the open-circuit voltage, $\frac{2.303RT}{nF\alpha}$ is the Tafel slope, i is the current density, and i_0 is the exchange current density for the ORR, n is the number of electron, F is the faraday constant and α is the symmetry factor. The kinetic parameters were obtained from I–V curves and Eq. (4).

The exchange current density, Tafel slope and symmetry factor are regarded as important kinetic parameters. The Tafel slope depends on α and n. The first charge transfer step is an electron transfer reaction (Eq. (5)) the number of electrons involved in which is given by the following equation [49]:

$$O_2 + H_3O^+ + e^- \xrightarrow{1} O_2H_{(ads)} + H_2O \tag{5}$$

In general, when the Tafel slope increases, the overpotential will increase faster with the current density. Thus, in an electrochemical reaction to obtain a high current at low over potential, the reaction should exhibit a low Tafel slope or large α. Exchanging the current density is an important kinetic parameter representing the electrochemical reaction rate at equilibrium. The exchange current density of an electrochemical reaction depends on the reaction and the electrode surface on which the electrochemical reaction occurs. Therefore, electrode materials or catalysts have a strong effect on ORR kinetics. Different materials can give different exchange current densities. Based on the LSV curve (Fig. 4A–C), GDE 231 in series 1 and GDE 103 in series 2 had low Tafel slope, high α, and high exchange current density. Therefore, these electrodes had the best performance for ORR in each series (Table 2). A comparison between catalysts 231, 103, and commercial Pt/C (Fig. 4C) shows that the activation of these synthesized catalysts for ORR is more efficient than commercial Pt/C. GDE 231 was found to have the best catalytic properties.

Oxygen permeability in electrodes

By using the chronoamperometry experiment and Cottrell equation the diffusion coefficient of oxygen at GDEs could be calculated [50]:

$$i = nFA(D/\pi t)^{1/2}C^* \tag{6}$$

where i is the limiting current (mA), n is the number of electrons, F is the Faraday constant (96485 $Cmol^{-1}$), A is the surface area of the electrode (cm^2), D is the diffusion coefficient (cm^2 s^{-1}), t is the time (s), and C^* is the concentration of the reactant.

The highest permeability value ($D^{1/2}C^*$) in series 1 and 2 were obtained for GDE 231 and GDE 103, respectively (Table 2). This result indicated that the diffusion of oxygen in the catalyst layer of these GDEs (231 and 103) was superior to other

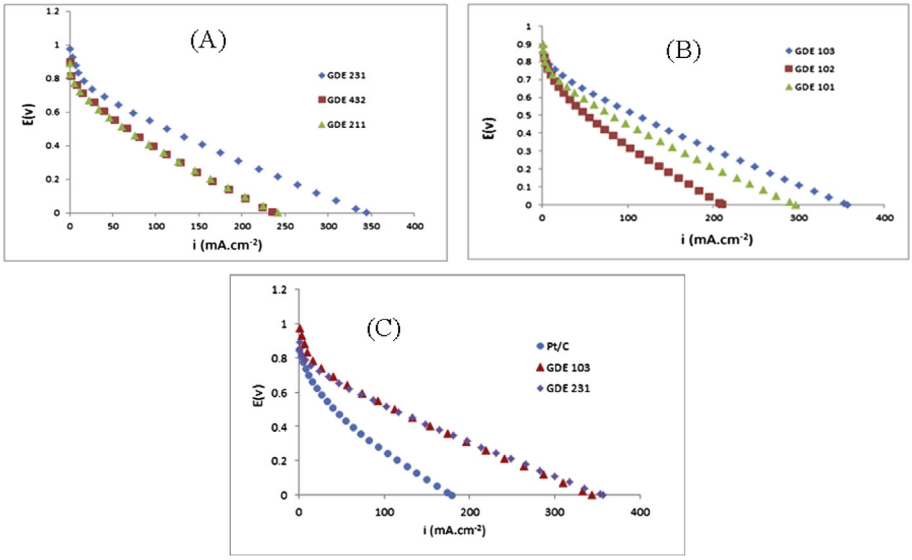

Fig. 4 – LSV curve for (A) series 1 electrodes (Ru@Pt–Pd) (231◊, 432□, 211Δ), (B) series 2 electrodes (Pd@Pt) (103◊, 102□, 101Δ) and (C) the comparison (Pt/C○, 103Δ, 231◊) in 0.5 M H_2SO_4, 5 mV s^{-1} scan rate and 25 °C.

catalysts, which improves the ORR in the mentioned GDEs. A comparison between these GDEs and commercial Pt/C demonstrated that both catalysts were more efficient than commercial Pt/C, with the 231 catalyst having the best permeability. This result could be attributed to the creation of appropriate substrate for oxygen diffusion to optimize oxygen consumption.

Impedance spectroscopy of fabricated electrodes

By using the impedance experiment in different condition we were able to determining the polarization and ionic resistance of GDEs. All results reported in Table 2.

To gain more information about the GDEs, the AC impedance spectrum of each GDE was obtained. The resulting data was plotted in the Nyquist representation. Although the impedance spectra had similar semi-circular shapes, the diameters of the semi-circles different significantly. As shown in Fig. 5A–C the charge transfer and Fig. 6A and B ionic resistance of GDE 231 in series 1 and GDE 103 in series 2 had minimum value. This result could be attributed to proper dispersion of catalyst nanoparticles and consequent formation of the three-phase zone in the catalyst layer. When the dispersion of catalyst and then the active surface area was enhanced, the charge transfer and ionic resistance were decreased. The semi-circle shapes of Nyquist plots point out to the equivalent circuit represented in Fig. 5D.

Study of single cell

As previously mentioned, the best catalyst of each series was used as cathode catalyst in the single cell. Polarization curve is the most important characteristic of a fuel cell. The polarization and power density curve of each single cell is reported in Figs. 7 and 8. The cells were tested under 3 different pressure values and two cathode humidification. Because the membrane requires proton conductivity, both reactant gases must be humidified before entering the cell. Needless to say, the proton was transferred from anode to cathode electrode with water. Water was also produced in the cathode reaction. Therefore, in order to avoided dryness of the membrane in the anode side, the gas (H_2) was 100% humidified. To avoid flooding in the cathode side, the gas humidification should be less than that in the anode side. In this research, 50% and 30% humidity was introduced into the cathode electrode. These results clearly indicated that the cell performance in these two conditions is not different (Figs. 7 and 8A and B). Therefore, it can be concluded that water management in our cells has been successful.

Increasing the gas pressure will enhance access to reactant species, resulting in an increase in the cell potential and performance (Table 3). There are two reasons for the improvement of performance by pressure: 1) It helps to remove the produced water from the cell. 2) It keeps the reactant concentration at a sufficiently high level. The power density of these cells is much higher compared with the alloy catalysts shown in other researches [34,35]. The single cell results indicated that the GDE 231 had better performance than the GDE 103 (Table 3). These results confirmed that the presence of Pd as alloy with Pt in shell and Ru in core improved the cell performance for ORR.

EIS experiments have been done at high current density region. Fig. 8 depicts the impedance spectra for PEM fuel cells in the Nyquist form at 0.3 V. In impedance spectra two semicircles at high and low frequency can be observed which are associated to the dynamics of charge and mass transfer, respectively [51]. The plot in Fig. 9 show the intersection of the imaginary impedance with the real impedance at high

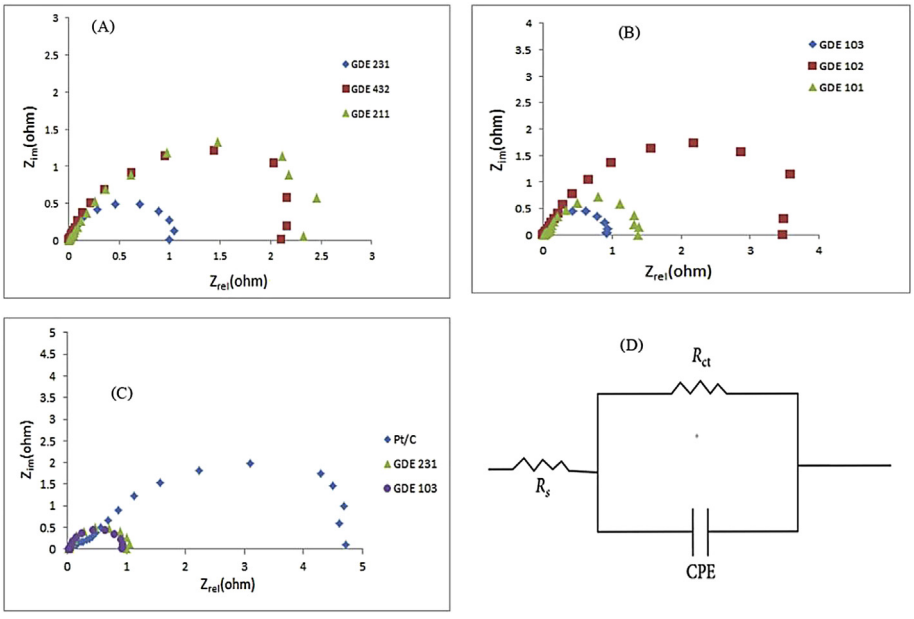

Fig. 5 – Nyquist plots of the impedance responses from 10 kHz to 100 mHz for (A) series 1 electrode (Ru@Pt–Pd) (231◊, 432□, 211Δ), (B) series 2 electrodes (Pd@Pt) (103◊, 102□, 101Δ) and (C) the comparison (Pt/C○, 103Δ, 231◊) in 0.5 M H_2SO_4, at 400 mV and 25 °C. (D) Equivalent circuit.

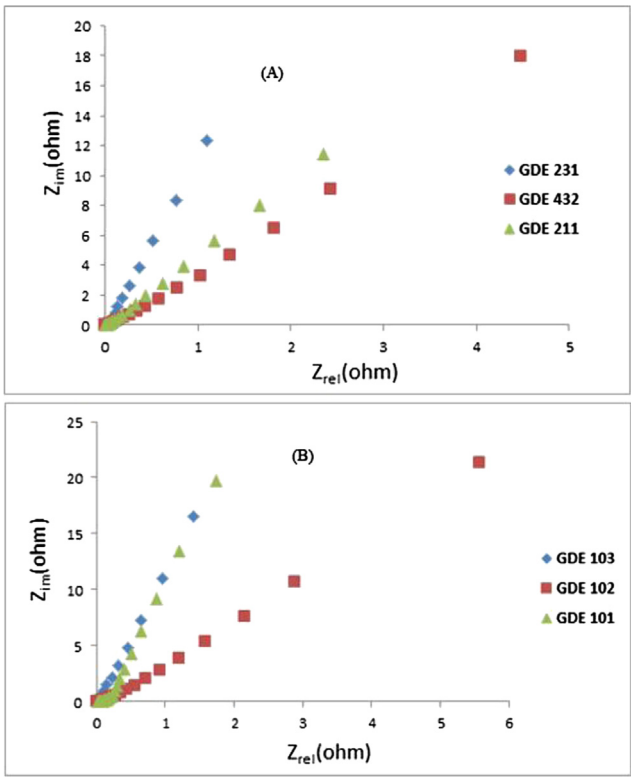

Fig. 6 – Nyquist plots of the impedance responses from 10 kHz to 100 mHz for (A) series 1 electrode (Ru@Pt–Pd) (231◊, 432□, 211Δ), (B) series 2 electrodes (Pd@Pt) (103◊, 102□, 101Δ) in 0.5 M H_2SO_4, at OCV, Ar atmospher and 25 °C.

frequencies shifts to the left. This result indicated a decrease in the PEM resistance with the change of cathode catalyst in cell. The change of impedance arc diameter due to mass transport process is negligible for using two different catalysts in cathode. The reason is related to the water management of the cell, thus mass transport limitation in two catalysts is the same.

In general, the electrochemical results of series 1indicated that the GDE 231 had maximum and the GDE 211 had minimum performance in ORR. Therefore, it could be concluded that in core-shell structure of Ru@Pt–Pd the 2:3:1 M ratio with 2.3 nm particle size and well dispersion of nanoparticle catalyst could be create vast three-phase zone. About the smaller particle size (2.1 nm in GDE 211) I should mention that the active surface area was low, therefore, the polarization resistance of GDE increased and subsequently the electrode performance decreased (Table 2). High ionic resistance of GDE 211 was demonstrated inadequacy of three-phase zone for ORR. In case of larger particles (2.9 nm in GDE 432), the effect of catalyst nanoparticles agglomeration reduced the oxygen diffusion coefficient as well as the electro active surface area (Table 2). Consequently, according to the obtained results, polarization and ionic resistance of this GDE has increased, while the current density is decreased.

The electrochemical results of series 2 indicated that the GDE 103 exhibited a maximum performance in this series (Table 2). Therefore, it can be concluded that in the core–shell structure of Pd@Pt the 1:0:3 M ratio of Pt, Ru, and Pd, respectively, had better performance than other molar ratios.

The comparison between the best electrodes of each series (GDE 103 and GDE 231) with commercial Pt/C indicated that the presence of Pd in the shell as alloy with Pt and Ru as core could improve the current density. Also the polarization resistance of GDE 231 was less than GDE 103 which is ascribed to improvement of output current density.

Finally, a comparison between the performance of GDE 103, GDE 231, and commercial Pt/C (10 wt%) reveals that the core–shell structure had better performance than the commercial Pt/C on ORR. It is also observed that these synthesized catalysts had a more electro active surface area and diffusion coefficient of oxygen as well as less polarization and ionic resistivity than the commercial Pt/C catalyst. The results of GDE 231 and GDE 103 were almost the same, but the GDE 231 had better performance in single cell.

The enhanced activity for ORR in catalyst 231 indicated that presence of Ru in core and Pt–Pd alloy in shell was able to improve the reduction of oxygen in PEMFC cathode. Both results in single cell and three-electrode system are attributed to

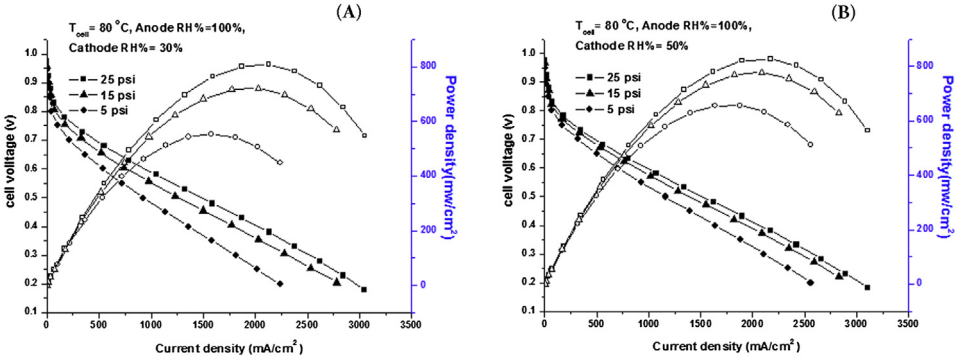

Fig. 7 – Polarization curves and power density of catalyst 231(Ru@Pt–Pd) in cathode and Pt/C in anode at different gas pressure o5, Δ15 and □25 psi, cell temperature 80 °C, anode RH = 100%, (A) cathode RH = 30% and (B) cathode RH = 50%, nyquist plots of cell at 300 mV, cell temperature 80 °C, gas pressure 25 psi, anode RH = 100%, (C) cathode RH = 30% and (D) cathode RH = 50%.

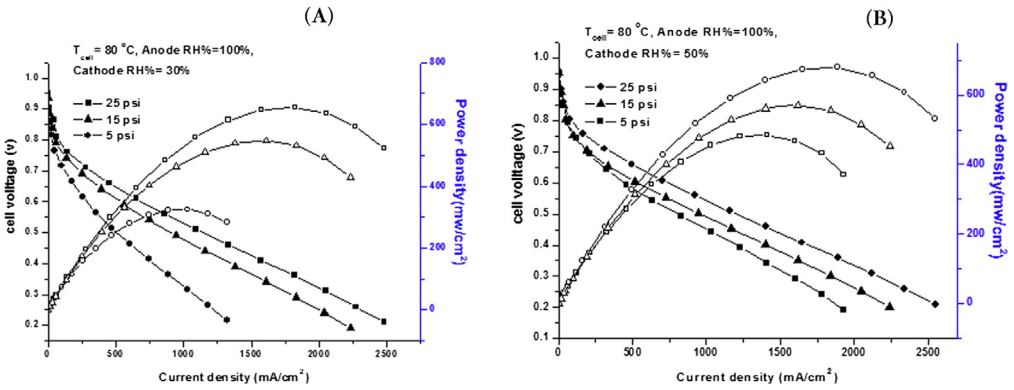

Fig. 8 – Polarization curves and power density of catalyst 103 (Pd@Pt) in cathode and Pt/C in anode at different gas pressure o5, Δ15 and □25 psi, cell temperature 80 °C, anode RH = 100%, (A) cathode RH = 30% and (B) cathode RH = 50%, nyquist plots of cell at 300 mV, cell temperature 80 °C, gas pressure 25 psi, anode RH = 100%, (C) cathode RH = 30% and (D) cathode RH = 50%.

Table 3 – Current density at 0.9 and 0.2 V and maximum power density of single cell for synthesized catalyst in MEA cathode.

Cathode catalyst for MEA	i at 0.9 V (mA cm^{-2})	Max. power density (mw cm^{-2})	i at 0.2 V (mA cm^{-2})	Max power density (w mg_{cat}^{-1})
231	28.9	830	3110	13.83
103	24.6	672	2550	11.20

the positive effect of Ru as core and Pd as alloyed with Pt in shell.

Because of electron transfer from Ru to Pt, therefore, the Fermi level shift to energy levels higher than pure Pt [52] and the oxygen absorption on Pt can be improved. In addition, the presence of Ru in the core will improve the chemical properties of Pt on shell which directly affects adsorption and reduction of oxygen on Pt catalyst [30,51]. On the other hand, the Pt–Pd alloy has been used for ORR in many studies, showing remarkable catalytic performance [11,15,53,21,54,34,35]. Thus, the application of Ru in core and Pt–Pd alloy in the shell can accelerate the ORR and consequently enhance the single cell performance. In spite of low catalyst loading (0.3 mg cm^{-2}), maximum power density of the catalyst 231 (830 mw cm^{-2}) is remarkably higher than that reported for Pt–Pd alloy in Ref. [35] (492 mw cm^{-2}) and [34] (322 mw cm^{-2}).

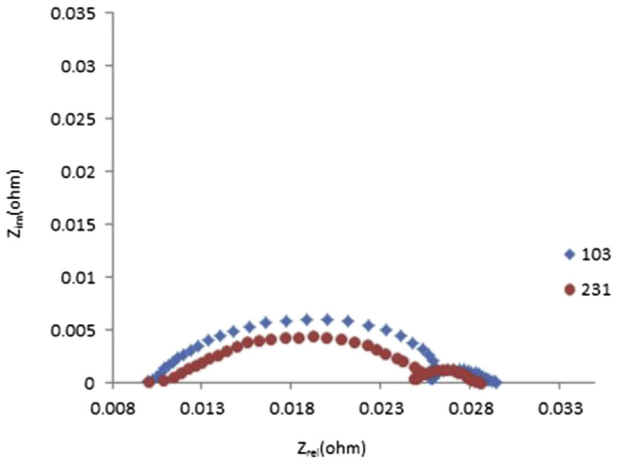

Fig. 9 – Nyquist plots at 0.3 V, 80□C, anode RH = 100%, cathode RH = 50% (○231, ◊103).

Conclusion

Because there are three kinds of species, namely gases, electrons and protons, which participate in the electrochemical reaction, the reaction can take place on the catalyst surface where they have access to all three species. The synthesized core–shell catalysts were prepared by using the impregnation and hydrothermal method with different molar ratios of differ metals. The physical properties and electrochemical performance of these electro catalysts were characterized using ICP, XRD, TEM, and a number of required electrochemical techniques. The ICP results revealed that the applied technique was proper for synthesizing core–shell structures. The XRD pattern and TEM images illustrate that the catalyst particles were nanometer-sized. The results of electrochemical experiment indicated that molar ratios of metals in the core and shell would affect the GDE performance so that in Pd@Pt the 1:3 for Pt: Pd and in Ru@Pt–Pd the 2:3:1 for Ru:Pt:Pd had the best performance in ORR for each series. In comparison with the best GDE of two series, the presence of Pd on shell (GDE 231) improved the electrode performance. Also, the comparison performance between GDE 103, GDE 231, and commercial catalyst (Pt/C 10% wt.) revealed that the core-shell structure improved the catalytic performance, while the presence of Ru in the core and Pd–Pt

alloy in the shell where observed to enhance the GDE performance compared with Pd as core and Pt as shell. The single cell results confirmed that the GDE 231 as cathode will improve the performance of PEMFC.

REFERENCES

[1] Thompson SD, Jordan LR, Forsyth M. Platinum electrodeposition for polymer electrolyte membrane fuel cells. Electrochem acta 2001;46:1657–63.

[2] Li WZ, Sun KQ, Hu Z, Xu BQ. Characteristics of low platinum Pt-BaO catalysts for NO_x storage and reduction. Catal Today 2010;153:103–10.

[3] Liu P, Wang J, Zhang X, Wei R, Ren X. Catalytic performances of dealuminated zeolite supported Pt catalysts doped with Cr in hydroisomerization of n-heptane. Chem Eng J 2008;148:184–90.

[4] Jahel A, Avenier P, Lacombe S, Fourcade JO, Jumas JC. Effect of indium in trimetallicPt/Al_2O_3SnIn-Cl naphtha-reforming catalysts. J Catal 2010;272:275–86.

[5] Matsumoto T, et al. Reduction of Pt usage in fuel cell electrocatalysts with carbon nanotube electrodes. Chem Commun 2004;7:840–1.

[6] Loganathan K, Bose T, Weinkauf D. Surface modification of carbon black by nitrogen and allylamine plasma treatment for fuel cell electrocatalyst. Int J Hydrogen energy 2014;39:15766–71.

[7] Liu Z, Ming Gan L, Hong L, Chen W, Lee JY. Carbon-supported Pt nanoparticles as catalysts for proton exchange membrane fuel cells. J power sources 2005;139:73–8.

[8] Moreira J, Angel del P, Ocampo AL, Sebastian PJ, Montoya JA, Castellanos RH. Synthesis, characterization and application of a Pd/Vulcan and Pd/C catalyst in a PEM fuel cell. Int J Hydrogen energy 2004;29:915–20.

[9] Yang H. Core-Shell and related multifunctional nanostructures of platinum-based electrocatalysts. Angew Chem Int Ed 2011;50:2674–6.

[10] Wang D, Li Y. Bimetallic nanocrystals: liquid-phase synthesis and catalytic applications. Adv Mater 2011;23:1044–60.

[11] Wang H, Xu C, Cheng F, Zhang M, Wang S, Jiang SP. Pd/Pt core–shell nanowire arrays as highly effective electrocatalysts for methanol electrooxidation in direct methanol fuel cells. Electrochem Commun 2008;10:1575–8.

[12] Guo SJ, Fang YX, Dong SJ, Wang E. High-efficiency and low-cost hybrid nanomaterial as enhancing Electrocatalyst: spongelike Au/Pt core/shell nanomaterial with hollow cavity. J Phys Chem C 2007;111:17104–9.

[13] Zeng JH, Yang J, Lee JY, Zhou WJ. Preparation of carbon-supported core–shell Au–Pt nanoparticles for methanol oxidation reaction: the promotional effect of the Au core. J Phys Chem B 2006;110:24606–11.

[14] Tena-Zaera R, Katty A, Bastide S, Levy-Clement C. Annealing effects on the physical properties of electrodeposited ZnO/CdSe core–shell nanowire arrays. Chem Mat 2007;19:1626–32.

[15] Yang JH, Zhou WJ, Cheng CH, Lee JY, Liu ZL. Pt-decorated PdFe nanoparticles as methanol-tolerant oxygen reduction electrocatalyst. ACS Appl Mater Interfaces 2010;2:119–26.

[16] Wang D, et al. Structurally ordered intermetallic platinum–cobalt core–shell nanoparticles with enhanced activity and stability as oxygen reduction electrocatalysts. Nat Mater 2013;12:81–7.

[17] Chen Y, Yang F, Dai Y, Wang W, Chen S. Ni@Pt core-shell nanoparticles: synthesis, structural and electrochemical properties. J Phys Chem C 2008;112:1645–9.

[18] Sarkar A, Manthiram A. Synthesis of Pt@Cu core-shell nanoparticles by galvanic displacement of Cu by Pt^{+4} ions and their application as electrocatalysts for oxygen reduction reaction in fuel cells. J Phys Chem.C 2010;114:4725–32.

[19] Koh S, Strasser P. Electrocatalysis on bimetallic surfaces: modifying catalytic reactivity for oxygen reduction by voltammetric surface dealloying. J Am Chem Soc 2007;129:12624–5.

[20] Whittingham MS, Savinell RF, Zawodzinski T. Introduction: batteries and fuel cells. Chem Rev 2004;104:4243–4.

[21] Zhang G, Shao ZG, Lu W. Core–shell Pt modified Pd/C as an active and durable electrocatalyst for the oxygen reduction reaction in PEMFCs. Appl Catal B: Environ 2013;132–(133):183–94.

[22] Wang H, Xu C, Cheng F, Zhang M, Wang S, Jiang SP. Pd/Pt core–shell nanowire arrays as highly effective electrocatalysts for methanol electro oxidation in direct methanol fuel cells. Electrochem Commun 2008;10:1575–8.

[23] Humbert MP, Smith BH, Wang Q, Ehrlich NS, Shao M. Synthesis and characterization of Pd –Pt core –Shell electrocatalysts for oxygen reduction. Electrocatal 2012;3:298–303.

[24] Zhang L, et al. Ti_4O_7 supported Ru@Pt core–shell catalyst for CO-tolerance in PEM fuel cell hydrogen oxidation reaction. Appl Energy 2013;103:507–13.

[25] Zhang Y, et al. Hollow core supported Pt monolayer catalysts for oxygen reduction. Catal Today 2013;202:50–4.

[26] Duan MY, Liang R, Tian N, Li YJ, Yeung ES. Self-assembly of Au–Pt core–shell nanoparticles for effective enhancement of methanol electro oxidation. Electrochim Acta 2013;87:432–7.

[27] Shimizu K, Cheng IF, Wai CM. Aqueous treatment of single-walled carbon nanotubes for preparation of Pt–Fe core–shell alloy using galvanic exchange reaction: selective catalytic activity towards oxygen reduction over methanol oxidation. Electrochem Commun 2009;11:691–4.

[28] Gao H, Liao S, Zeng J, Xie Y, Dang D. Preparation and characterization of core–shell structured catalysts using Pt_xPd_y as active shell and nano-sized Ru as core for potential direct formic acid fuel cell application. Electrochim Acta 2011;56:2024–30.

[29] Anastasijevic NA, Dimitrijevic ZM, Adzic RR. Oxygen reduction on a ruthenium electrode in acid electrolytes. Electrochem Acta 1986;31:1125–30.

[30] Prakash J, Joachin H. Electrocatalytic activity of ruthenium for oxygen reduction in alkaline solution. Electrochim Acta 2000;45:2289–96.

[31] Lischka M, Mosch C, Gro A. Tuning catalytic properties of bimetallic surfaces: oxygen adsorption on pseudomorphicPt/Ruoverlayers. Electrochim Acta 2007;52:2219–28.

[32] Inoue H, Brankovic SR, Wang JX, Adzic RR. Oxygen reduction on bare and Pt monolayer-modified Ru(0001), Ru(1010)and Ru nanostructured surfaces. Electrochim Acta 2002;47:3777–85.

[33] Limpattayanate S, Hunsom M. Electrocatalytic activity of Pt-Pd electrocatalysts for the oxygen reduction reacti on in proton exchange membrane fuel cells: effect of supports. Renew Energy 2014;63:205–11.

[34] Thanasilp S, Hunsom M. Effect of Pt: Pd atomic ratio in Pt-Pd/C eletrocatalyst-coated membrane on the electrocatalytic activity of ORR in PEM fuel cells. Renew Energy 2011;36:1795–801.

[35] Zhang J, Vukmirovic MB, Xu Y, Xu Y, Mavrikakis M, Adzic RR. Controlling the catalytic activity of platinum-monolayer electrocatalysts for oxygen reduction with different substrates. Angew Chem 2005;117:2170–3.

[36] Gharibi H, Javaheri M, Mirzaie RA. The synergy between multi-wall carbon nanotubes and Vulcan XC72R in microporous layers. Int J Hydrogen energy 2010;35:9241–51.

[37] Gharibi H, Javaheri M, Kheirmand M, Mirzaie RA. Optimization of the amount of Nafion in multi-walled carbon nanotube/Nafion composites as Pt supports in gas diffusionelectrodes for proton exchange membrane fuel cells. Int J Hydrogen energy 2011;36:13325–34.
[38] Lefebvre MC, Martin RB, Pickup PG. Characterization of ionic conductivity profiles within proton exchange membrane fuel cell gas diffusion electrodes by impedance spectroscopy. Electrochem Solid-State Lett 1999;2(6):259–61.
[39] Qi Z, Lefebvre MC, Pickup PG. Electron and proton transport in gas diffusion electrodes containing electronically conductive proton-exchange polymers. J Electroanal Chem 1998;459:9–14.
[40] Saab AP, Garzon FH, Zawodzinski TA. Determination of ionic and electronic resistivities in carbon/polyelectrolyte fuel-cell composite electrodes. J Electrochem Soc 2002;149:1541–6.
[41] Barbir FPEM. fuel cells: theory and practice. Elsevier Inc; 2005p 93.
[42] Zhao H, Li L, Yang J, Zhang Y. Co@Pt–;Ru core-shell nanoparticles supported on multiwalled carbon nanotube for methanol oxidation. Electrochem Commun 2008;10:1527–9.
[43] Lust E, Härk E, Nerut J, Vaarmets K. Pt and Pt–Ru catalysts for polymer electrolyte fuel cells deposited onto carbide derived carbon supports. Electrochimica Acta 2013;101:130–41.
[44] Wang W, Wang RF, Ji S, Feng H, Wang H, Lei Z. Pt overgrowth on carbon supported Pd Fe seeds in the preparation of core–shell electrocatalysts for the oxygen reduction reaction. J Power Sources 2010;195:3498–503.
[45] Wang C, et al. Multimetallic Au/FePt3 nanoparticles as highly durable electrocatalyst. Nano Lett 2011;11:919–26.
[46] Pozio A, Francesco MD, Cemmi A. Comparison of high surface Pt/C catalysts by cyclic voltammetry. J Power Sources 2002;105:13–9.
[47] Bockris JO'M. Modern electro chemistry. 2nd ed. Plenum; 2000p. 1054.
[48] Beattie PD, Basura VI, Holdcroft S. Temperature and pressure dependence of O_2 reduction at Pt Nafion® 117 and Pt BAM® 407 interfaces. J Electroanal Chem 1999;468:180–92.
[49] Wang J. Analytical electrochemistry. 2nd ed. Wiley; 2000p. 60.
[50] Yaun X, Song C, Wang H, Zhang J. Electrochemical impedance spectroscopy in PEM fuel cell fundamentals and applications. Springer, New York, USA. 2010p. 263.
[51] Kang DB, Lee CK. Electronic properties of Ru/Pt(111) Alloy surface: a theoretical study of H_2O adsorption. Bull Korean Chem Soc 2000;21(1):87–92.
[52] Jakob P, Schlapka A, Gazdzicki P. Oxygen adsorption on Pt/Ru(0001) layers. J Chem Phys 2011:134 (224707-1)-(224707-10).
[53] Wang H, Wang R, Li H, Wang Q, Kang J, Lei J. Facile synthesis of carbon-supported pseudo-core@shell PdCu@Pt nanoparticles for direct methanol fuel cells. Int J hydrogen energy 2011;36:839–48.
[54] Trinh QT, Yang J, Lee JY, Saeys M. Computational and experimental study of the volcano behaviour of the oxygen reduction activity of PdM@PdPt/C (M = Pt, Ni, Co, Fe, and Cr) core–shell electrocatalysts. J Catal 2012;291:26–35.

Update

International Journal of Hydrogen Energy
Volume 40, Issue 33, 7 September 2015, Page 10704

DOI: https://doi.org/10.1016/j.ijhydene.2015.06.092

Available online at www.sciencedirect.com

ScienceDirect

journal homepage: www.elsevier.com/locate/he

Corrigendum

Corrigendum to "Investigating the influence of Pd situation (as core or shell) in synthesized catalyst for ORR in PEMFC" [Int J Hydrogen Energy 40 (2015) 6661–6671]

M. Javaheri[*]

Ceramic Department, Materials and Energy Research Center, Karaj, Iran

The author regrets the omission of the following acknowledgment in the published article, and apologizes for any inconvenience caused:

The work reported here was supported by Iran National Science Foundation (INSF).

DOI of original article: http://dx.doi.org/10.1016/j.ijhydene.2015.03.030.

* Tel.: +98 912 5263035.

E-mail addresses: m.javaheri@merc.ac.ir, javaheri54@yahoo.com.

http://dx.doi.org/10.1016/j.ijhydene.2015.06.092